Journal of Instrumentation

Study of the single cluster response of a helium-isobutane drift chamber prototype using 8 keV X-rays

PUBLISHED BY IOP PUBLISHING FOR SISSA MEDIALAB

RECEIVED: *October 31, 2014*
REVISED: *December 10, 2014*
ACCEPTED: *January 27, 2015*
PUBLISHED: *March 11, 2015*

Study of the single cluster response of a helium-isobutane drift chamber prototype using 8 keV X-rays

G. Cavoto,[a] **S. Dabagov,**[b,c] **D. Hampai,**[d] **G. Piredda,**[a] **F. Renga,**[a,1] **E. Ripiccini,**[a,e] **C. Voena**[a] **and A. Zullo**[a]

[a] *INFN Sezione di Roma, Piazzale A. Moro 2, 00185 Roma, Italy*
[b] *RAS, P.N. Lebedev Physical Institute, Moscow, Russia*
[c] *National Research Nuclear University MEPhI, Moscow, Russia*
[d] *INFN Laboratori Nazionali di Frascati, Via E. Fermi 40, 00044 Frascati, Italy*
[e] *Dipartimento di Fisica dell'Università "Sapienza", Piazzale A. Moro 2, 00185 Roma, Italy*

E-mail: francesco.renga@roma1.infn.it

ABSTRACT: The identification of single clusters in the electronic signals produced by ionizing particles within a drift chamber is expected to significantly improve the performances of this kind of detectors in terms of particle identification capabilities and space resolution. In order to develop refined cluster recognition algorithms, it is essential to measure the response of the chamber and its electronics to single ionization clusters. This can be done by irradiating the chamber with X-rays. We report here on the studies performed on a drift chamber prototype for the MEG-II experiment at the X-ray facility of the INFN Frascati's National Laboratories "XLab Frascati". The prototype is operated with a helium-isobutane mixture and instrumented with high bandwidth custom pre-amplifiers. The results of this study have been used to develop an innovative method for cluster recognition, based on the Wiener filter technique, which has been tested on data collected at the Frascati's Beam Test Facility. As a side measurement, we also performed a study of the gas gain in a configuration which is similar to that of the MEG-II experiment.

KEYWORDS: Wire chambers (MWPC, Thin-gap chambers, drift chambers, drift tubes, proportional chambers etc); Pattern recognition, cluster finding, calibration and fitting methods; Performance of High Energy Physics Detectors; Charge transport and multiplication in gas

ARXIV EPRINT: 1410.8719

[1] Corresponding author.

doi:10.1088/1748-0221/10/03/P03012

Contents

1 Introduction

In the development of gaseous detectors, and, in particular, of drift chambers, it is necessary to study the generation of the signals produced by ionizing particles in the adopted gas admixture and electric field configuration, and to determine the response of the front-end electronics to these signals. This is crucial in order to validate the design of the chamber, and to determine its expected performances through reliable simulations. An X-ray source, used to irradiate a drift chamber prototype reproducing the design of the final detector, is the ideal tool to fulfill this task.

Charged particles ionizing a gas admixture produce clusters of a few electron-ion pairs at different locations along their path. In a drift chamber, the electrons in a cluster drift together toward an anode wire, where an ionization avalanche occurs, with a characteristic multiplication factor per electron (*gas gain*). In this way, each cluster produces an individual signal in the chamber (*single-cluster signal*), but the observed waveform will be indeed a superposition of several single-cluster signals.

Conversely, photo-electric effect by an X-ray produces a single electron, which carries, in the first approximation, all the energy of the incident X-ray. This electron having a few keV kinetic energy flies at most a few hundred microns in a typical drift chamber gas admixture, before losing all the energy by further ionizations, and eventually thermalizes. It results in a cluster of electron-ion pairs localized within ~ 1 mm of the X-ray interaction point. The average number of pairs is also proportional to the X-ray energy. We used the software DEGRAD v2.5 [1] to simulate these processes, assuming a $He : C_4H_{10}$ (89:11) mixture. Figure 1 shows the position of the electrons produced in a typical event, and the distribution of the number of electrons produced by 8.5 keV X-rays. Although the total extent of the electron cloud can be significantly large, most of the electrons tend to concentrate in a few clusters, well separated in space, resulting into consecutive signals well separated in time. Hence, in several cases, an X-ray will produce signals very similar, in shape, to

2015 JINST 10 P03012

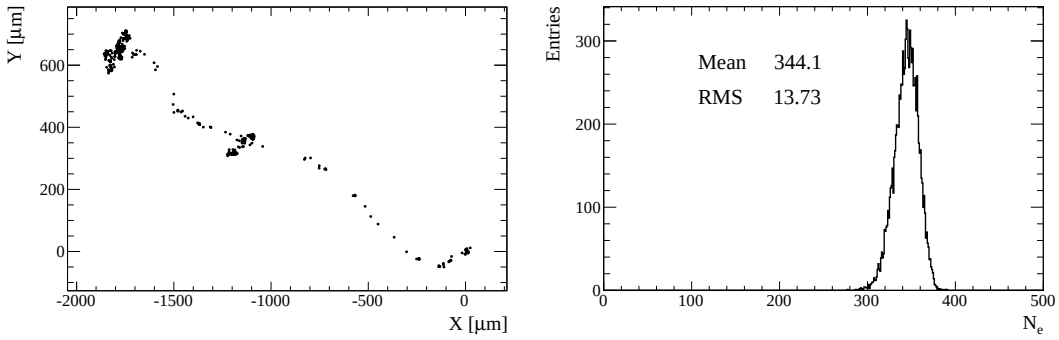

Figure 1. Results of a DEGRAD simulation in a He : C_4H_{10} (89:11) mixture. Left: position of the electrons produced in a typical event by a single 8.5 keV X-ray ionizing the gas at the origin of the reference system. Right: distribution of the number of electrons for a set of events.

the single-cluster signals produced by a charged particle, although sometimes multiple clusters can show up. Moreover, the average integrated charge will be proportional to the average number of pairs (i.e. to the X-ray energy) and to the gain of the chamber. In conclusion, measuring both the charge and shape of the signals produced by X-rays allows measuring the gain of the chamber (if the X-ray energy spectrum is known) and determining the shape of single-cluster signals. These two inputs allow, for instance, the front-end electronics to be optimized, the working conditions of the chamber to be determined (in order to avoid significant aging due to the large amount of collected charge), and reliable simulations to be developed. This will be of paramount importance for the development of the Monte Carlo simulation for the MEG-II experiment.

The knowledge of the signal shape is even more important in the development of drift chambers with single-cluster detection capabilities, which are expected to significantly improve the performances of this kind of detector by providing the number of ionization clusters for particle identification purposes (*cluster counting*) [2, 3] and the drift time of each single cluster for position reconstruction purposes (*cluster timing*) [4]. Indeed, refined algorithms can be developed for the identification of clusters in the signal waveforms, if the single-cluster signal shape is well known.

We exploited the X-ray test facility (XLab Frascati) [5] of the INFN Frascati's National Laboratories (LNF) to study the signals of a drift chamber prototype. Compared to ^{55}Fe X-ray sources, this facility provided high rates in a safe environment, thanks to its intense and collimated beam. Moreover, the higher energy of X-rays at XLab Frascati ($\sim$ 8 keV from Cu emission lines) improved the signal over noise ratio. The collected data allowed to develop new cluster identification algorithms, based on the Wiener filter technique [6], and study the cluster counting capabilities of our device.

2 The drift chamber prototype

The prototype under test, built as an R&D project for the MEG-II experiment [7], is described in detail in [8]. It is constituted by a gas-tight Aluminum body of $20 \times 20 \times 50\,\mathrm{cm}^3$. The lateral faces are made of 1.5 mm thick Al plates and/or 50 μm thick aluminized kapton windows, depending on the set-up. The other two faces are closed by two end-plates made of Au-plated Al and drilled to

2015 JINST 10 P03012

accomodate the feedthroughs where the wires were soldered and the gas pipe fittings. The hole mask defines a 8×8 array of 7 mm-side square cells, each with a sense wire (25 μm Au-plated Tungsten) in the middle and 8 field wires (80 μm Au-plated Tungsten wires) all around.

The prototype is instrumented with custom large-bandwitdh preamplifiers in order to improve its single cluster recognition capabilities. The gain of the amplifier is approximately 600 mV/fC. Further details can be found in [7].

The high voltage, positive with respect to the ground, is supplied to the sense wires through a 1 kHz RC low-pass filter, and distributed to each wire through a 10 MΩ resistance. In order to avoid signal reflections, the impedance of the high voltage boards on the wire side is adapted to match the cell impedance, measured to be $\sim 330\,\Omega$.

3 Single cluster and gain measurement at XLab Frascati

The XLab Frascati has a 4 m^3 shielded cabinet to host the detector or the sample to be irradiated. Inside the cabinet, an Oxford Apogee 40 W X-ray tube with Cu target is placed that can be moved horizontally and vertically with millimetric precision. The drift chamber prototype has been positioned inside the cabinet so that the X-rays impinge perpendicularly on one of the long sides and enter the chamber through the 50 μm aluminized Kapton window, which has been mounted to avoid an excessive X-ray attenuation. The vertical position of the tube with respect to the cell has been scanned to maximize the event rate. The high voltage was supplied to the sense wire of the irradiated cell and its surrounding wires. The data have been taken with both a 6-channel and a 1-channel versions of the pre-amplifier. The amplified signal from the irradiated cell is read-out with a high bandwidth differential probe to a 1 GHz bandwidth, 10 GS/s oscilloscope (LeCroy WaveRunner 610Zi).

3.1 The X-ray source

The voltage of the source has been chosen to be 25 kV which provides good Cu emission lines ($K_{\alpha 1} = 8.04778$ keV, $K_{\alpha 2} = 8.02783$ keV, $K_{\beta 1} = 8.90529$ keV) over a broad background, as shown in figure 2. The current of the tube can be varied to regulate the X-ray intensity. It was scanned between 5 and 25 μA, but most of the measurements were done at 5 μA, which is assumed through the paper unless explicitly stated. The intensity of the source at the origin was $\sim 10^8$ γ/s. Taking into account the attenuation in air, kapton and gas before reaching the instrumented cell, and the expected ionization probability in the 7 mm of gas within the cell, a signal rate of about 10–100 kHz was expected.

3.2 Single cluster signals

In the coaxial approximation, the current signal produced in a drift chamber by the avalanche initiated by a single electron has the characteristic form [9]

$$I(t) \propto \frac{1}{t + t_0}\,, \tag{3.1}$$

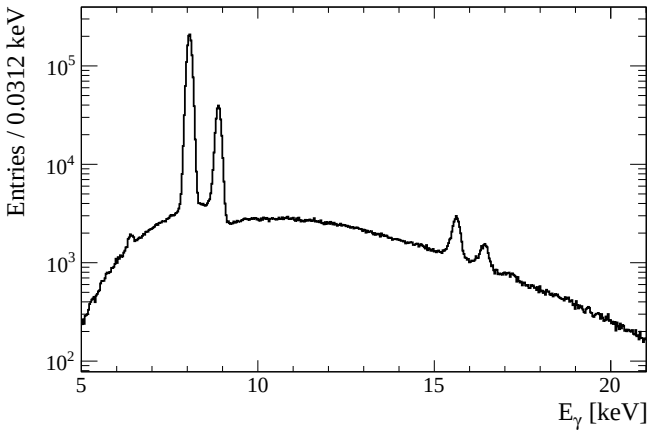

Figure 2. Emission spectrum of the X-ray tube used at XLab Frascati, under the operating conditions adopted during the drift chamber prototype tests. The first peak results from the superposition of the two K_α lines.

where the time constant t_0 depends on the ion mobility μ and the electrical configuration of the drift cell. In particular, for the n-th wire

$$\frac{1}{t_0} = \frac{\mu}{a^2 \pi \epsilon_0} \left(\sum_{m=1}^{N} c_{nm} U_m \right) , \tag{3.2}$$

where a is the sense wire radius, N is the number of wires, c_{nm} is the capacitance matrix of the wire grid and U_m the voltage of the wires. When the ions produced in the avalanche reach the field wires, after a time $t_{\max}$, the signal stops. Hence, the normalization of $I(t)$ in eq. (3.1) is given by the condition

$$Q_{\text{tot}} \equiv \int_0^{\infty} I(t)\, dt = \int_0^{t_{\max}} I(t)\, dt = G \cdot q_e \, , \tag{3.3}$$

where G is the gas gain and q_e the electron charge The mobility for several ions in helium can be found in literature [10]; although a reference for the mobility of isobutane ions in helium could not be found, according to the available measurements a reasonable range for our setup is 10–20 $\text{cm}^2\text{V}^{-1}\text{s}^{-1}$. The capacitance matrix has been estimated by means of analytical calculations within GARFIELD. As a result, we obtain $t_0 = 0.150$–0.300 ns and $t_{\max} = 8$–$16\,\mu$s for a voltage of 1560 V. Considering that the chamber has been operated within a $\pm 10\%$ voltage range around this value, and μ is expected to be relatively stable with respect to the isobutane fraction, we do not expect significant differences of this shape through the configurations under test.

The current signal is then amplified by the front-end electronics, resulting in a voltage signal

$$V(t) = \int_0^{t_{\max}} w(t - t')\, I(t')\, dt \, , \tag{3.4}$$

where $w(t - t')$ is the electronics response to an infinitely fast unit charge signal (*delta response*).

To measure the response of the chamber (including the electronics contribution) to the X-ray single clusters an average of the acquired signals has been performed. First of all, we rescaled all waveforms to unit amplitude and aligned their starting time, taken at the half-maximum of the

leading edge. Then, we removed signals that saturated the oscilloscope acquisition (~ 680 mV) and signals whose full-width at half-maximum indicated the presence of multiple clusters (see figure 3). Finally, a bin-by-bin average of the waveform amplitudes is taken in a range of 100 ns (1000 sampling bins) around the signal. To further remove a small fraction of noisy signals, waveforms deviating from the average signal by more than 4 standard deviations in more than 10 sampling bins were also removed. The results were shown to be stable with respect to small changes of the selection criteria.

Figure 4 shows the superposition of the waveforms, normalized to their maximum amplitude. The dark line represents the average response. Two different configurations have been tested:He : C_4H_{10} (89:11) mixture with 1-channel pre-amplifier and He : C_4H_{10} (93:7) mixture with 6-channel amplifier are shown.

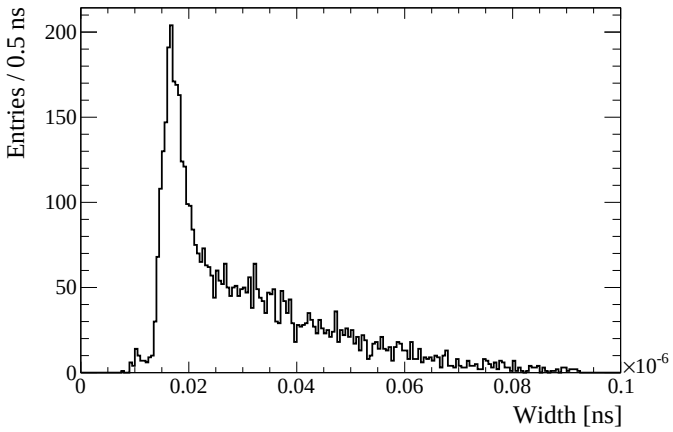

Figure 3. Distribution of the full-width half-maximum of collected X-ray signals. A large full-width half-maximum was found to be associated to events with multiple clusters clearly visible in the signal waveform. In order to have a pure sample of single-cluster events, only waveforms with a full-width half-maximum between 15 and 20 ns are used.

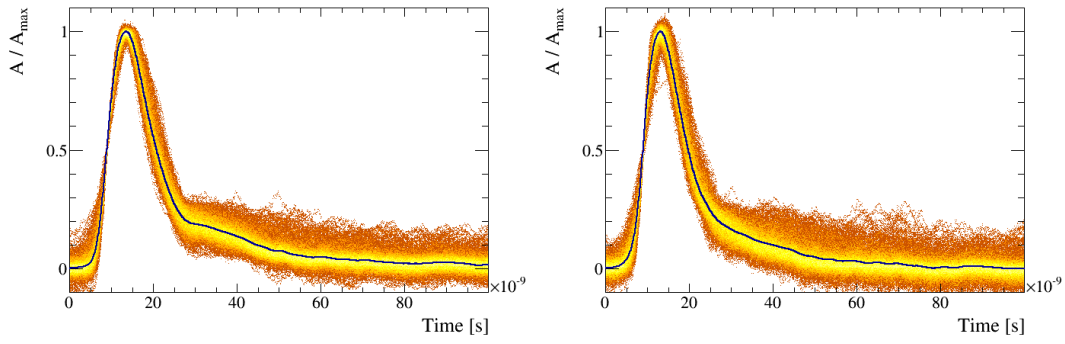

Figure 4. Superposition of single cluster waveforms. Left: He : C_4H_{10} (89:11) mixture with 1-channel pre-amplifier. Right: He : C_4H_{10} (93:7) mixture with 6-channel amplifier. Point density is larger in the lighter-colored regions. The dark line represents the average.

The shape is very similar, with small dependence on the high voltage and the mixture. Some difference is observed between the two pre-amplifiers, which could be due to a known impedance mismatch in the 1-channel preamplifier. The long tail expected from the slow ion drift is observed. The above response functions can be used in the MEG-II simulations and as signal templates in cluster counting/timing studies.

3.3 Gain measurement

As a side measurement, we also tested a method for the gain measurement using X-rays. A reliable estimate of the gain is indeed crucial for the choice of the working point of drift chambers operating in a high rate environment, as in MEG-II, in order to avoid intolerable aging effects due to an excessive charge collection.

Considering that the cluster produced by an X-ray contains an average of N_e electrons, we can write the Gain G as

$$G = \frac{Q_{\text{tot}}}{N_e q_e} \,. \tag{3.5}$$

The charge of the collected signals has to be estimated from the integral of the voltage signals in a 100 ns window. In this case, no selection is applied on the full-width half-maximum in order to collect all the charge released in the event, while an algorithm based on the single cluster templates has been used to get a correct estimate of the charge also for the saturated signals.

Figure 5 shows the signal integrals for the He : C_4H_{10} (89:11) mixture with different high voltages and 1-channel preamplifier. As expected, at higher high voltages, the average charge is higher. The width of the distribution is also increasing with the high voltage as it increases with the gain.

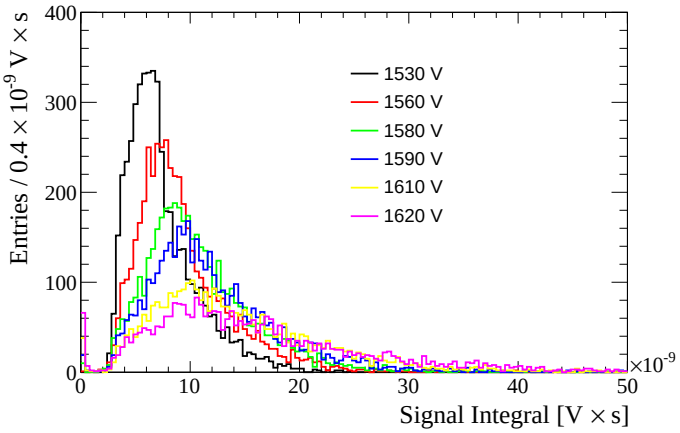

Figure 5. Signal integrals $\mathscr{I}_{\text{meas}}$ (in V × s) in a 100 ns window for different high voltages. The mixture is He : C_4H_{10} (89:11). The signals are readout with the 1-channel preamplifier.

A scan of the tube current has been performed up to 25 μA, while the working point used for all other measurements is 5 μA. Figure 6 shows the integrated charge distribution and the variation of the charge mean value as a function of the tube current. The mean value is corrected according to the expected gain vs. high voltage curves (see below), to take into account the voltage drop across

the high voltage supply circuit of the prototype. Nonetheless, a decrease at higher tube current is observed, that may be due to space charge effects appearing at high rate. An exponential fit is used to extrapolate the integral to $I = 0$, and indicates a 9% gain suppression at 5 μA with respect to the zero-current limit.

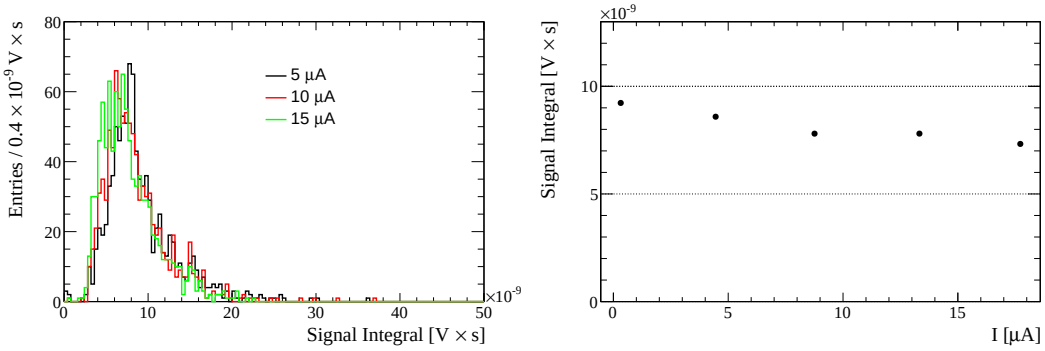

Figure 6. Left: signal integrals $\mathscr{I}_{\text{meas}}$ (in V $\times$ s) in a 100 ns window for the He : C_4H_{10} (89:11) mixture, HV = 1560 V, 1-channel preamplifier and different currents of the X-ray tube. Right: mean value of the integral distribution versus tube current.

In order to extract a charge measurement from the signal integrals, two factors need to be considered: the response of the front-end electronics and the loss of the charge in the long signal tails due to the limited integration window. Calculations based on the coaxial approximation of section 3.2 give an expected $(43 \pm 4)\%$ charge loss for t_0 ranging from 0.150 to 0.300 ns. From eq. (3.4), the measured signal integral can be written as

$$\mathscr{I}_{\text{meas}} = \int_0^T V(t)\,dt = \int_0^T dt \int_0^{t_{\max}} w(t-t')I(t')\,dt' = \int_0^{t_{\max}} dt' I(t') \int_0^{T-t'} dt'' w(t''), \quad (3.6)$$

with T = 100 ns. Once the electronics response $w(t)$ is known, the integral can be performed numerically and the ratio of Q_{tot} to $\mathscr{I}_{\text{meas}}$, which is independent of G, can be used as a conversion factor to transform the signal integral into a collected charge. It accounts for both the limited integration window and the electronics response, which has been extracted from a circuit simulation including the preamplifier, the drift chamber equivalent circuit and the HV board. A conversion factor of 2.1×10^{-3} (3.0×10^{-3}) $\frac{C}{V \times s}$ has been found for the 1-channel (6-channel) pre-amplifier.

We also need to take into account the combined effect of the time distribution of the secondary electron clusters produced by the X-rays (section 1), the space charge felt by clusters reaching the sense wire with a significant delay and the oscilloscope trigger threshold (124 mV). A waveform simulation, driven by the results of DEGRAD, GARFIELD, and a study of the space charge effect on waveforms produced by charged tracks, has been used to model these effects and revealed a 35 to 45% underestimate of the true gain, increasing with the gain itself.

With all these calibration, a measurement of the average gain can be extracted from the signal integral distribution. For this purpose, the X-ray spectrum of figure 2 has been convolved with a Gaussian response function and multiplied by a threshold function, and then fitted to the measured spectra. Only the gain and the width of the Gaussian response are floating in the fit. The fitted gas gain as a function of the high voltage is shown in figure 7. A 34% systematic error, fully corre-

2015 JINST 10 P03012

lated among the data points, is included in the plot (gray belt). It accounts for the three dominant sources of uncertainty: the pre-amplifier calibration (± 30%, estimated from the differences in the calibrated response of different amplifiers under the same data taking conditions), the correction factor from waveform simulations (± 15%, estimated by variating the simulation inputs) and the t_0 value used to extract the expected charge loss (± 9%). The results are also compared with a GARFIELD simulation which reproduces the geometrical and electrical configuration of the prototype, and takes into account the gas properties by performing a microscopic simulation of the avalanche process initiated by thermalized electrons. A satisfactory agreement is found.

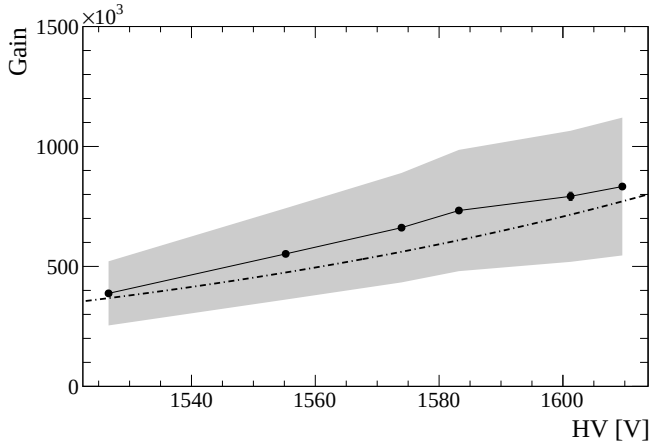

Figure 7. Gas gain as a function of the drift chamber high voltage for the He : C_4H_{10} (89:11) mixture. The gray belt shows the systematic uncertainties described in the text. The predictions of a GARFIELD simulation are given by the dashed line.

4 A Wiener filter approach for cluster counting

The Wiener filter technique is widely used for the deconvolution of a known delta response from a signal affected by noise. If the underlying signal is assumed to be a Dirac delta-function, the result of the deconvolution is a narrow peak at the signal leading edge, and it makes possible to resolve near signals. Hence, this technique is promising also for searching single clusters in the signal produced by a charged particle within a drift chamber.

Given the noise spectrum and the expected single-cluster signal template, we consider a Wiener filter defined by the following response function in the frequency domain

$$H(\nu) = \frac{S^*(\nu)}{|S(\nu)|^2 + |N(\nu)|^2}\,, \tag{4.1}$$

where $S(\nu)$ and $N(\nu)$ are the Fourier transform of the single-cluster signal template and the average Fourier transform of the noise, respectively. Compared to the corresponding pure Fourier deconvolution, $H(\nu) = S^*(\nu)/|S(\nu)|^2$, the Wiener deconvolution efficiently suppresses the noise, but the peaks in the filtered waveform get wider. Conversely, compared to another popular kind of optimum filter, defined by $H(\nu) = S^*(\nu)/|N(\nu)|^2$, the noise suppression in less efficient. In order

to optimize the filter for cluster identification, we adopted this response function as a compromise

$$H(\nu) = \frac{S^*(\nu)}{|S(\nu)|^2 + k^2|N(\nu)|^2}\,, \tag{4.2}$$

where k is a factor to be optimized, while $S(\nu)$ is extracted considering the average signal amplitude. We apply the filter to the collected waveform $W(t)$, by means of Fast Fourier Transforms $\mathscr{F}$, according to

$$\widetilde{W}(t) = \mathscr{F}^{-1}\{H(\nu)\cdot\mathscr{F}\{W(t)\}\} \tag{4.3}$$

and a cluster emerges in the filtered waveform $\widetilde{W}(t)$ as a narrow peak at the leading time of the single-cluster signal. It can be identified looking for local maxima in the filtered waveform, separated from local minima by more than n times the noise RMS measured in the filtered waveform itself, where n has also to be optimized (clusters are searched for in a range of $[-50,+200]$ ns around the leading edge of the signal, defined as the time at which the signal exceeds 3 times the noise RMS).

The Wiener filter method has been first applied to simulated waveforms in order to test its theoretical capabilities. In a first simulation we assumed a Gaussian, 2 mV RMS noise and an ideal signal shape with a very short rise time (~ 2 ns), a $1/t$ tail, and an average amplitude of 30 mV per cluster. Cluster times are simulated according to the expectations for the geometry of our prototype. The performances of the algorithm are evaluated in terms of cluster recognition efficiency and probability of a cluster of not being a fake (*purity*), and compared to the results obtained with a general purpose peak-finding algorithm [11]. Several combinations of n and k have been tried, and the best ones have been chosen for the comparison. The same approach is adopted to find the best combinations of parameters for the general purpose algorithm. The results are shown in figure 8. The Wiener filter approach, being tailored on the expected single cluster waveforms, clearly outperforms the general purpose algorithm.

In order to test the capabilities of the Wiener filter technique on real data, we exploited a set of data collected with our prototype at the LNF Beam Test Facility (BTF) [8, 12]. We used an electron beam with 447 MeV/c in energy, a rate of 25 Hz and an average of one particle per spill. About 4 m behind the prototype there was a calorimeter which allowed to count the number of electrons per spill (we selected events with only one electron) and provided the track time to be used in the the drift chamber reconstruction. The chamber was operated with the $He : C_4H_{10}$ (89:11) mixture at 1620 V. The 6-channel preamplifier was used to readout some of the cells in a horizontal row. The signals from the pre-amplifiers were sent to a board which converted them in single-ended mode. The single-ended signals were digitized by a high bandwidth (1 GHz) digitization board [13].

Figure 9 shows the average noise spectrum and the average frequency spectrum of waveforms with a reconstructed hit. Thanks to the measurements performed at XLab Frascati, we can use the single cluster template to build the Wiener Filter, along with this noise spectrum. The results of a simulation generated according to the signal template measured at XLab Frascati and the noise observed at BTF are also shown in figure 8. The part of the envelope curve with highest purity comes from $k \sim 5$ and $n > 4$. Hence we used $k = 5$ to build the filter and $n = 4$ for cluster identification in the filtered waveform. Figure 10 shows an example of waveform with the identified clusters.

For our 7 mm cell we expect about 12 clusters on average, given that the mean free path for cluster production, estimated from GARFIELD simulations, is 0.6 mm. The distribution of the

2015 JINST 10 P03012

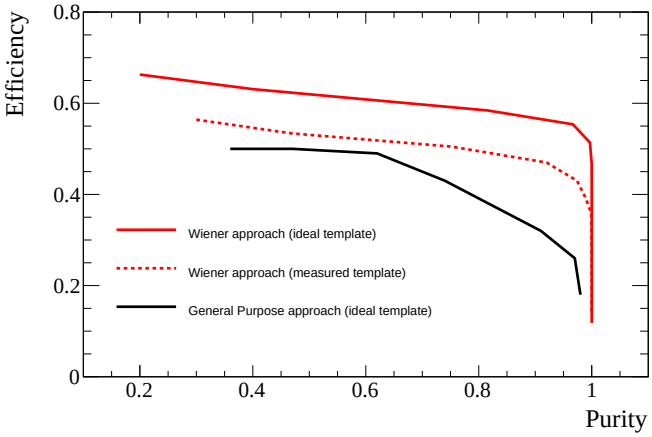

Figure 8. Performances of the Wiener filter approach (red) for simulated ideal signals (rise time ~ 2 ns), compared to the performances obtained from the general purpose peak-finding approach described in [11] (black). For each method, the curve is obtained by varying all the parameters and taking the envelope of the resulting curves. The results of a simulation based on the measured template and noise are also shown (dashed red).

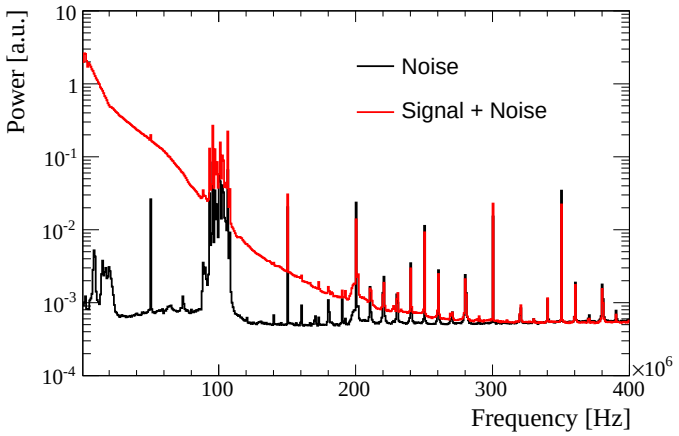

Figure 9. Average frequency spectrum of the noise (black) and signal plus noise (red) waveforms at BTF.

number of identified clusters is shown in figure 11. The average (~ 3.3) suggests an efficiency around 30%, considering that for $n \geq 4$ most of our simulations give only a few percent of fake clusters. It has to be compared with an efficiency of $\sim 50\%$ obtained in the simulation.

Many effects are expected to reduce the number of identified signals, and in particular:

1. the gas gain fluctuations, which are typically large in a gas chamber, and can make a fraction of signals to be below the noise level — this is expected to significantly improve in future applications, where better electromagnetic shielding and grounding schemes will be adopted;

2. the gain suppression induced on subsequent clusters by the space charge of the first avalanches — a reduced noise level will also allow to recover part of this inefficiency;

2015 JINST 10 P03012

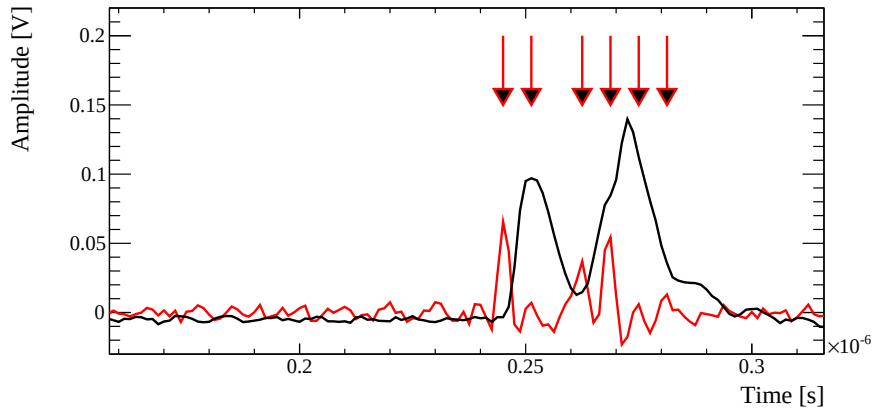

Figure 10. Segment of a BTF signal waveform $W(t)$ (black) with the result $\widetilde{W}(t)$ of the filter from eq. (4.3) super-imposed (red, arbitrarily normalized) and the identified clusters indicated by arrows. Notice that the filter is built in such a way that peaks show up at the leading edge of the cluster signal.

3. the shape of the single-cluster signal, namely its finite rise and fall times, originating from both the time development of the avalanche and the limited bandwidth of the readout electronics, which prevents to resolve very close clusters.

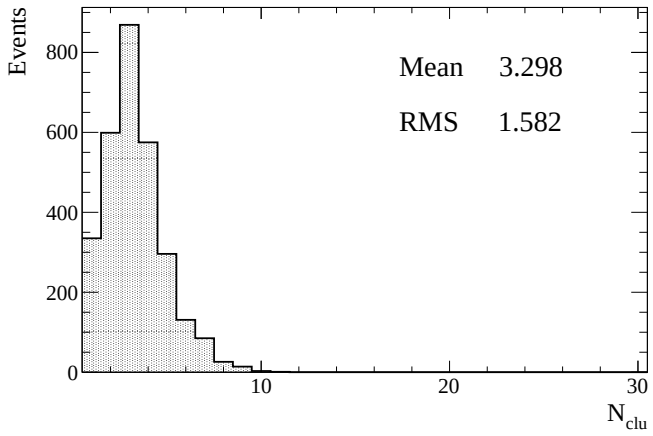

Figure 11. Number of identified clusters per cell and event in BTF data.

5 Conclusions

We have studied the single cluster response of a drift chamber prototype to 8 keV X-rays at the XLab Frascati of the INFN Frascati's National Laboratories. We obtained the response of the chamber and the electronics to single clusters, a fundamental input for developing refined cluster counting/timing techniques. We also developed a method to measure the chamber gain in our configuration. Thanks to these data, a novel algorithm for cluster identification, based on a Wiener filter, has been developed and preliminarily tested on data collected at the Frascati's Beam Test Facility.

Acknowledgments

We thank V. Bocci, R. Lunadei, D. Ruggieri and our colleagues of the MEG-II collaboration for the kind support in the construction and operation of the drift chamber prototype used for this study, and we are grateful to the BTF crew for the support during the beam tests in Frascati. We also thank S. Biagi and R. Veenhof for the support in the use of the DEGRAD software. S. Dabagov would like to acknowledge the support by the Ministry of Education and Science of RF in the frames of Competitiveness Growth Program of NRNU MEPhI, Agreement 02.A03.21.0005. F. Renga and C. Voena acknowledge the support from MIUR (grant RBFR138EEU_001/I18C13000090001).

References

[1] http://consult.cern.ch/writeup/magboltz/.

[2] A. Davidenko et al., *Measurements of the relativistic increase of the specific primary ionization in a streamer chamber*, *Nucl. Instrum. Meth.* **67** (1969) 325.

[3] J.F. Caron et al., *Improved particle identification using cluster counting in a full-length drift chamber prototype*, *Nucl. Instrum. Meth.* **A 735** (2014) 169.

[4] G. Tassielli et al., *Improving spatial resolution and particle identification*, *Nucl. Instrum. Meth.* **A 572** (2007) 198.

[5] http://www.lnf.infn.it/xlab/index.html.

[6] H. Wiener, *Extrapolation, Interpolation, and Smoothing of Stationary Time Series*, John Wiley and Sons Inc., New York U.S.A. (1949).

[7] A.M. Baldini et al., *MEG Upgrade Proposal*, arXiv:1301.7225.

[8] A.M. Baldini et al., *Measurement of single hit resolution of the MEG-II drift chamber prototypes*, paper in preparation.

[9] W. Blum, W. Riegler and L. Rolandi, *Particle Detection with Drift Chamber*, Springer-Verlag, Heidelberg Germany (2008).

[10] W. Lindinger and D.L. Albritton, *Mobilities of various mass-identified positive ions in helium and argon*, *J. Chem. Phys.* **62** (1975) 3517.

[11] M. Morhac et al., *Identification of peaks in multidimensional coincidence gamma-ray spectra*, *Nucl. Instrum. Meth.* **A 443** (2000) 108, the implementation within the ROOT data analysis framework has been used.

[12] http://www.lnf.infn.it/acceleratori/btf/.

[13] D. Breton, E. Delagnes and J. Maalmi, *Using ultra fast analog memories for fast photodetector readout*, *Nucl. Instrum. Meth.* **A 695** (2012) 61.

2015 JINST 10 P03012